Fatigue Crack Paths in Sintered Duplex Stainless Steels

F. Iacoviello[1], V. Di Cocco[1], M. Cavallini[2], T. Marcu[3] and A. Molinari[3]

[1] Università di Cassino, Di.M.S.A.T., via G. Di Biasio 43, 03043 Cassino (FR) ITALY, iacoviello@unicas.it
[2] Università di Roma "La Sapienza", I.C.M.M.P.M., via Eudossiana 18, 00184 Roma ITALY, mauro.cavallini@uniroma1.it
[3] Università di Trento, Dip. Ing. dei Materiali, Via Mesiano 77, 38050 Trento ITALY, Alberto.Molinari@ing.unitn.it

ABSTRACT. *Duplex stainless steels (DSSs) are in between the austenitic and the ferritic grades, combining the best mechanical and corrosion resistance properties of both. As a result of their high mechanical strength, good thermal conductivity and excellent corrosion resistance, DDSs are extensively used both in pulp and paper industries, in chemical and petrochemical plants. They also find some applications in food and biomedical fields as well. The high chromium (between 21 and 27 wt.%) and molybdenum (up to 4.5 wt.%) contents allow the use of DSSs under conditions of pitting, crevice and, above all, stress corrosion cracking that would be critical for the traditional AISI 304 and 316. Finally, some economic advantages follow as a result of lower nickel content than the austenitic grades. Fatigue crack propagation in duplex stainless steels is strongly affected by microstructure and therefore by the choice of the steel grade or by the heat treatment conditions. In the present work we considered three different sintered duplex stainless steels. Their fatigue crack propagation resistance was investigated by means of fatigue crack propagation tests according to ASTM E 647 standard, considering three different stress ratios ($R = K_{min}/K_{max}$). Crack surfaces were extensively analysed by means of a scanning electron microscope. Crack paths were investigated by means of a crack path profile analysis performed by means of an optical microscope. In order to analyse phases volume fractions and micropores influence, da/dN-ΔK fatigue crack propagation results were compared with profile an fracture surface analysis.*

INTRODUCTION

Austenitic-ferritic (duplex) stainless steels are becoming more and more popular for many applications in chemical, petrochemical, nuclear and food industries. This is due to their combination of high mechanical properties and excellent localised corrosion resistance in neutral and acidic containing solutions, with a Ni content that is lower than austenitic grades with analogous generalised and localised corrosion resistance levels [1-4]. Numerous microstructural changes can occur in duplex stainless during isothermal or anisothermal heat treatments [5-7], above 1050°C (a steel ferritisation

with a ferrite/austenite volume fraction increasing), between 1050 and 600°C (corresponding to the precipitation of numerous carbides, nitrides and intermetallic phases with kinetic behaviour that is strongly affected by the stainless steel chemical composition) and between 600 and 300°C (with the ferrite spinodal decomposition and the precipitation of other intermetallic phases). These steels are characterised by some difficulties from the manufacturing point of view. Powder metallurgy could be an alternative to produce these steels, although it is not optimised up to now [8].

The aim of the present work is to analyse the fatigue crack propagation resistance of sintered duplex stainless steels and the investigation of the microstructure influence on fatigue crack propagation micromechanisms.

MATERIALS AND EXPERIMENTAL METHODS

Three different sintered duplex stainless steels were considered, obtained from the mixing of austenitic AISI 316LHC and ferritic AISI 434LHC stainless steels powders (table 1-2). Two different powder volume fractions were investigated (e.g. V_f = Ferrite powder volume/ Austenite powder volume = 0.67 and 0.43). Furthermore, for the same powder volume fraction (V_f = 0.43), two different sintered stainless steel densities were investigated (e.g. ρ [g/cm^3] = 6.89 and 7.12). Tables 1-2 show stainless steels powders chemical composition.

Table 1. AISI 316LHC austenitic stainless steel powder chemical composition.

C	Mo	Ni	Mn	Cr	Si
0.019	2.28	12.75	0.17	16.3	0.87

Table 2. AISI 434LHC ferritic stainless steel powder chemical composition.

C	Mo	Ni	Mn	Cr	Si
0.016	1.03	-	0.18	16.57	0.70

Sintering was performed at 1250°C under vacuum, for 1 hour. The sintering duration is not sufficiently long to get a complete homogenization of the material [9]. As a consequence, between the two constituents a zone of diffusion is formed in which the Ni content is intermediate (from 3 to 9%). During the cooling operation, three phases are obtained with volume fractions that depend on the powder volume fractions as follows:

Considering: V_f = 0.67 (60% AISI 316LHC + 40% AISI 434LHC)
%Austenite = 31.0 %
%Ferrite = 7.5 %
%Martensite = 61.5 %

Considering: $V_f = 0.43$ (70% AISI 316LHC + 30% AISI 434LHC)
%Austenite = 48.9 %
%Ferrite = 11.6 %
%Martensite = 39.5 % .

Metallographic samples were prepared and etching was carried out with Beraha reagent (0.7 g $K_2S_2O_3$, 20% HCl). The quantitative characterization of the microstructure was performed by an Image Analysing System. The microstructures of the investigated materials consists of mixtures of ferrite, martensite and austenite, as indicated in Figs 1 and 2. The corresponding percentages measured by Image Analysis were specified previously.

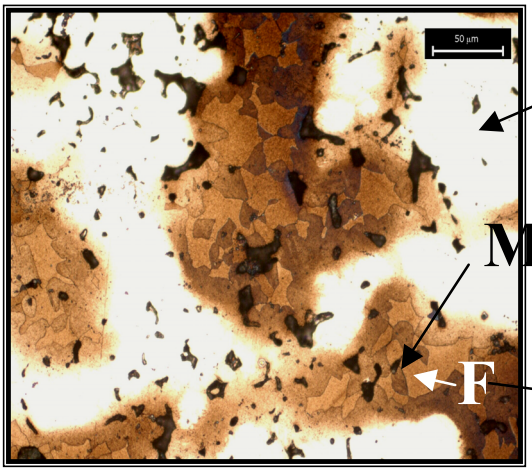

Figure 1. 60%316L+40%434L.

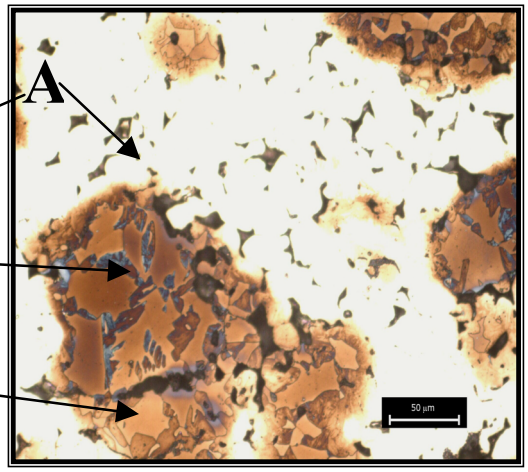

Figure 2. 70%316L+30%434L.

Density and porosity were measured by Archimede's method. Microhardness was measured on each constituent of the microstructure. Hardness HV30 represents the average of the values obtained considering three samples each material.

Three point bending test was carried out on an Instron machine, at room temperature. In order to determine the transverse rupture strength (TRS), 5 samples of 30mmx10mmx6mm each material were tested.

Fatigue tests were run according to ASTM E647 standard [10], using CT (Compact Type) 10 mm thick specimens and considering three different stress ratio values (e.g. $R = P_{min}/P_{max} = 0.1; 0.5; 0.75$). Tests were performed using a computer controlled Instron 8501 servohydraulic machine in constant load amplitude conditions, considering a 30 Hz loading frequency, a sinusoidal waveform and laboratory conditions. Crack length measurements were performed by means of a compliance method using a double cantilever mouth gage and controlled using an optical microscope (x 40). Fracture surfaces were analysed by means of a Philips scanning electron microscope (SEM). Fatigue crack path analysis was conducted considering all the fractured specimens, by means of an optical microscope (x200), according to the following procedure:

- Fracture surface nickel coating (in order to protect fracture surface during cutting);

- Fractured specimen longitudinal cutting, at half thickness, along the fatigue crack propagation direction (by means of a diamond saw);
- Metallographic preparation of the section (up to 0.2 μm Al_2O_3 powder)
- Chemical attack performed in a $CuCl_2$ (2g) + HCl (40 ml) + ethanol (40 ml) solution for about 15-30 seconds.

RESULTS AND DISCUSSION

The microhardness HV0.01 of the three phases are given in Table 3. Hardness HV30 and TRS of the studied materials are given in Table 4. As expected, hardness and TRS decrease by increasing the austenite percent, as can be observed in Table 4.

Table 3. Microhardness of the constituent phases in the studies materials

Material	*HV0.01 austenite*	*HV0.01 ferrite*	*HV0,01 martensite*
60%316L+40%434L	147	188	236
70%316L+30%434L	138	184	226

Table 4. HV30 and TRS of the studied materials

Material	*HV30*	*TRS [MPa]*
60%316L+40%434L	134	925
70%316L+30%434L	112	790

Stress ratio influence on the investigated sintered duplex stainless steels fatigue crack propagation is shown in Figs 3 to 5. All the investigated sintered duplex stainless steels show the influence of the crack closure effect [11, 12]: the higher the stress ratio R value, the lower the ΔK_{th} values are. Furthermore, for the same ΔK values, a crack growth rate da/dN values increase is obtained with the increasing of R values.

Considering the two investigated powder volume fractions (0.67 and 0.43), and considering the sintered stainless steel variability in da/dN-ΔK fatigue data [13, 14], fatigue crack propagation results show that the powder volume fractions influence is really low.

On the other hand, the influence of the steel densities is more evident for lower R values (R = 0.1). The higher the density, the lower is the fatigue crack propagation rate, especially in the stage II of III (Paris stage). In stage I of III (threshold stage) and in the stage III of III (final rupture), the density influence is less evident.

SEM fracture surface analysis shows that fatigue crack propagation micro-mechanisms do not depend on R values or on the applied ΔK conditions. Furthermore, the same fatigue crack propagation micro-mechanisms are observed for all the investigated stainless steel, although, probably, the importance of the different micro-mechanisms could be dependent on phases volume fraction and density. For example,

considering the always the same loading conditions (Figs 6, 8, 10; R = 0.1; ΔK = 15 MPa√m), SEM fracture surface analysis shows both ductile and fragile striations are probably corresponding to austenite and ferrite zones respectively (Fig. 6). Micropores could act as stress raisers: as a consequence both secondary cracks and cleavage fractures could develop (Fig. 8). Furthermore, microductility is observed (Fig. 10).

Austenitic and ferritic powder volume fraction, and the consequent phases volume fractions, seems to have a certain influence, although lower then the steel density. The optical microscope fatigue crack path analysis performed on the three investigated sintered steels for all the considered loading conditions shows that crack path is substantially independent from the loading conditions (R and ΔK values). Furthermore, for all the investigated steels (Figs 7, 9, 11; R = 0.1; ΔK = 15 MPa√m), micropores appear to not play the role of preferential fatigue path. The main deviations from the pure mode I fatigue crack propagation are connected to the ferrite/austenite interfaces, where the martensite presence is really important, with a consequent fracture surface roughness increase. These interfaces are the preferential, but not unique, fatigue crack paths for all the investigated sintered steel in all the considered loading conditions. As a consequence, martensite influences the fatigue crack propagation resistance according with two different concurrent mechanisms:

- considering its lower toughness, martensite plays the role of preferential fatigue crack path with a consequent fatigue crack growth rate increase;
- considering the evident crack path deviations from the pure mode I, its presence implies an increase of the importance of the roughness induced crack closure effect; this influence is more evident for lower R values.

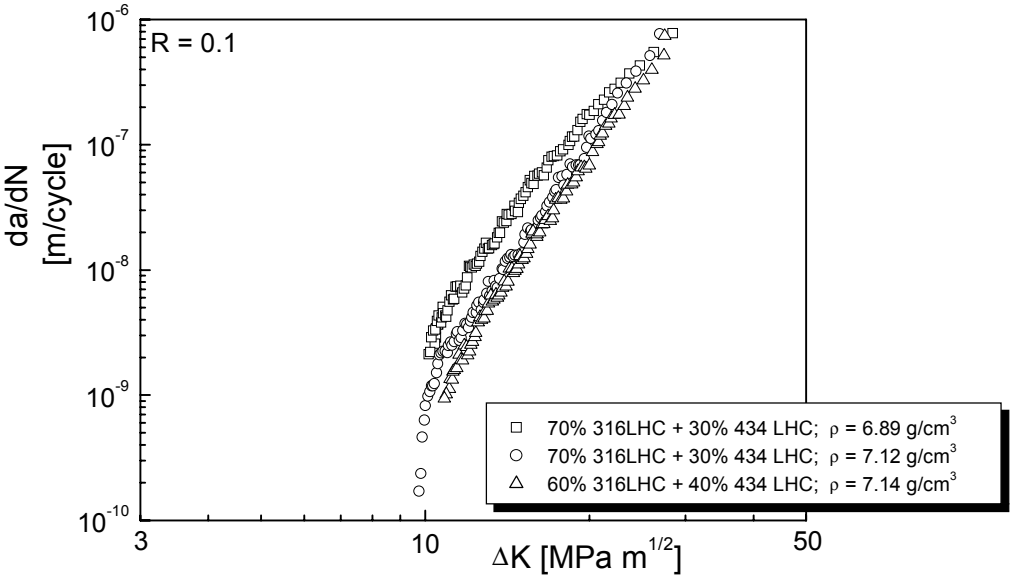

Figure 3. Fatigue crack propagation results for the investigated sintered duplex stainless steels (R = 0.1).

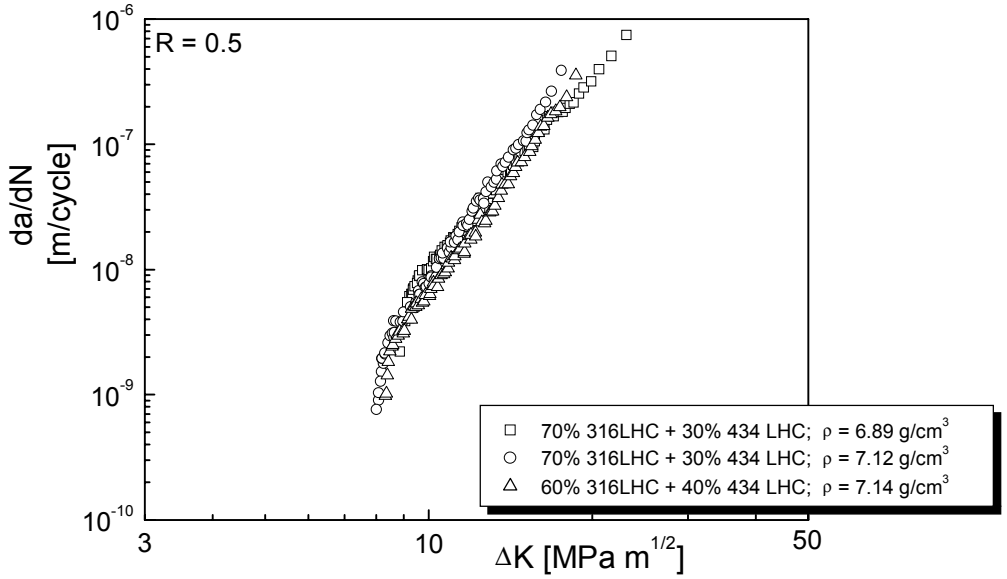

Figure 4. Fatigue crack propagation results for the investigated sintered duplex stainless steels (R = 0.5).

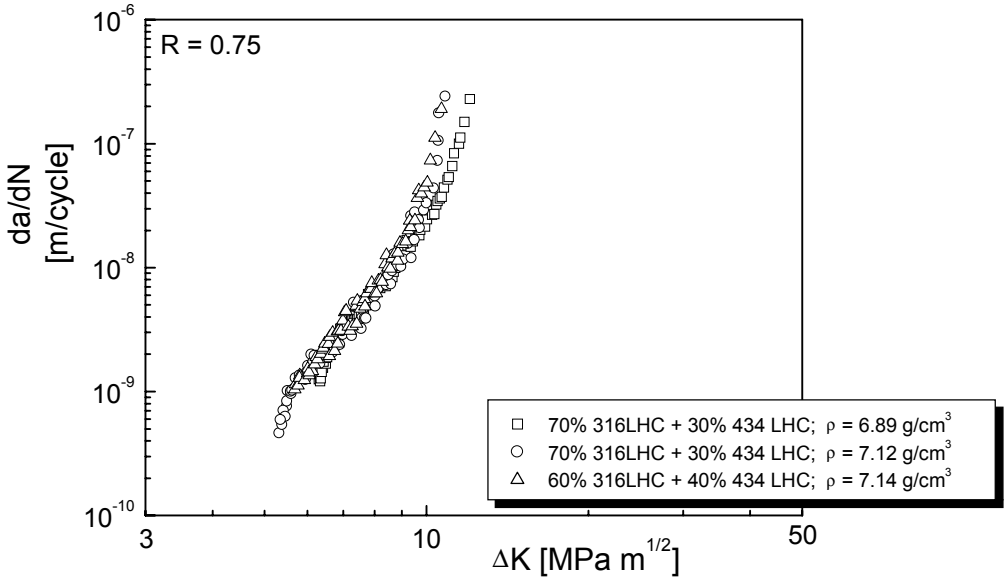

Figure 5. Fatigue crack propagation results for the investigated sintered duplex stainless steels (R = 0.75).

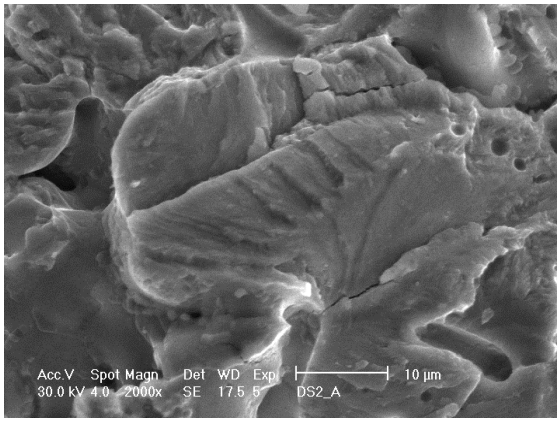

Figure 6. 70% AISI 316LHC + 30% AISI 434 LHC (ρ = 6.89 g/cm^3) SEM fracture surface analysis.

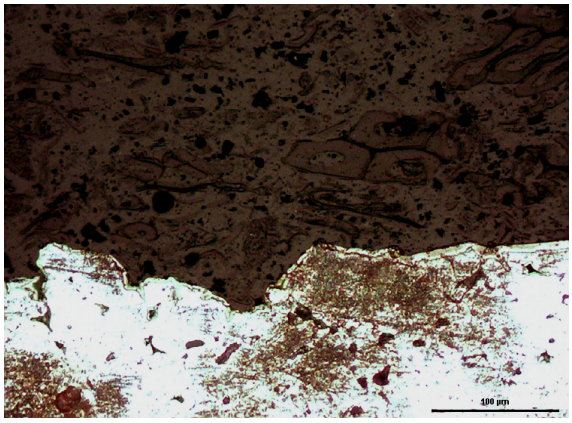

Figure 7. 70% AISI 316LHC + 30% AISI 434 LHC (ρ = 6.89 g/cm^3 optical microscope fatigue crack path analysis.

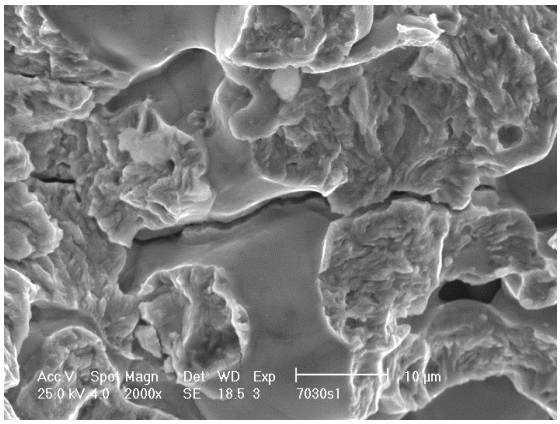

Figure 8. 70% AISI 316LHC + 30% AISI 434 LHC (ρ = 7.12 g/cm^3) SEM fracture surface analysis.

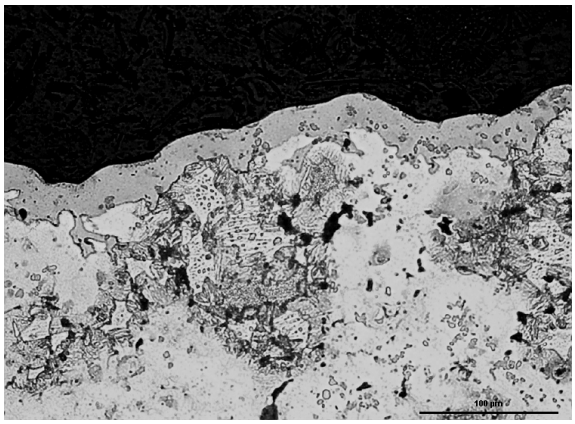

Figure 9. 70% AISI 316LHC + 30% AISI 434 LHC (ρ = 7.12 g/cm^3) optical microscope fatigue crack path analysis.

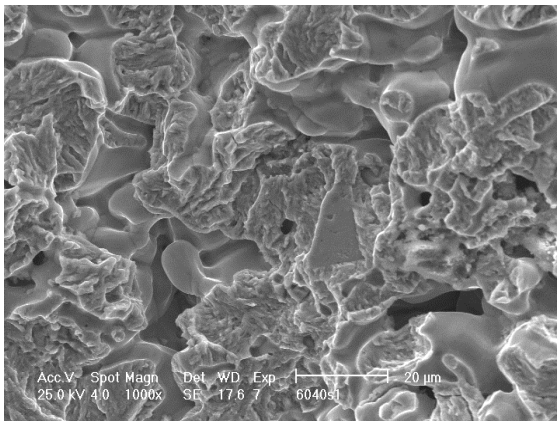

Figure 10. 60% AISI 316LHC + 40% AISI 434 LHC (ρ = 7.14 g/cm^3) SEM fracture surface analysis.

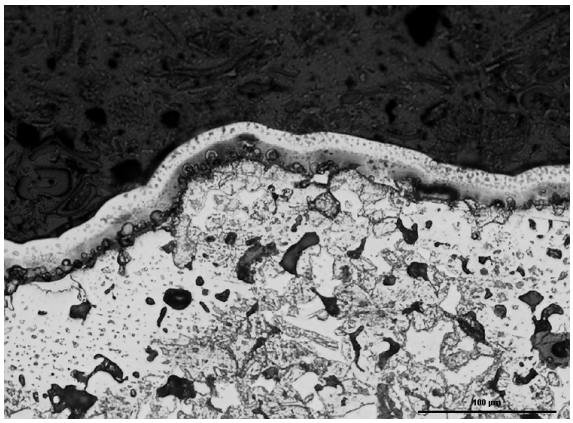

Figure 11. AISI 316LHC + 40% AISI 434 LHC (ρ = 7.14 g/cm^3) optical microscope fatigue crack path analysis.

CONCLUSIONS

Experimental results allow to summarize the following considerations:
- Considering higher R values, da/dN-ΔK fatigue crack propagation results are almost independent from the powders volume fraction and from the density; considering lower R values, the higher the steel density, the lower the fatigue crack growth rate (da/dN) is.
- Also fatigue crack propagation micromechanisms are independent from the loading conditions.
- Fatigue crack path analysis shows an evident influence of the martensite. This fragile phase constitutes a path for the preferential fatigue crack propagation.

On the basis of the experimental results it is possible to conclude that the increase of the fatigue crack propagation resistance of sintered stainless steels obtained from a mixing of AISI 316LHC and AISI 434 LHC, needs both a density increase and the decrease of the martensite volume fraction, in order to reduce both the influence of micropores and the possibility for the crack to find a preferential path.

REFERENCES

1. Bernhardsson, S. (1991) *Duplex stainless steel 91*, Beune, Francia, Les édition de physique, 185-199.
2. Charles, J. (1991) *Duplex stainless steel 91*, Beune, Francia, Les édition de physique, 3-45.
3. Gunn, R.N. (1997) *Duplex Stainless Steels – Microstructure, properties and applications*, Abington Publishing, Cambridge, England,.
4. Lacombe, P., Baroux, B. and Beranger, G. (1990) *Les aciers inoxydables*, Les éditions de physique.
5. Guttmann, M. (1991) *Duplex stainless steel 91*, Beune, Francia, Les édition de physique, 79-87.
6. Redjamia, A., Metauer, G. and Gantois, M. (1991) *Duplex stainless steel 91*, Beune, Francia, Les édition de physique, 119-128.
7. Josefsson, B., Nilsson, J.O. and Wilson, A. (1991) *Duplex stainless steel 91*, Beune, Francia, Les édition de physique, 68-78.
8. Datta, P. and Upadhyaya, G.S. (2001) *Materials Chemistry and Physics* **67**, 234–242.
9. Molinari, A., Marcu Puscas, T. and Straffelini, G. (2001) *La Metallurgia Italiana* **6**, 29-33.
10. *ASTM Standard test Method for Measurements of fatigue crack growth rates (E647-93)*, Annual Book of ASTM Standards (1993), Vol. 0301, American Society for Testing and Materials.
11. Elber, W. (1971), *ASTM STP 486*, 280.
12. Ritchie, R.O. and Suresh, S. (1982) *Metall. Trans. A* **13A**, 937.
13. Iacoviello, F., Di Cocco, V., Cavallini, M. and Molinari, A. (2002) *Proc. XXIX Convegno AIM*, Modena (Italy), n. 153.
14. Iacoviello, F. (2000) *International Journal of Fatigue* **22**, 657-663.